IEEE Access
Multidisciplinary | Rapid Review | Open Access Journal

Received 1 November 2023, accepted 8 December 2023, date of publication 18 December 2023,
date of current version 26 December 2023.

Digital Object Identifier 10.1109/ACCESS.2023.3344093

RESEARCH ARTICLE

D-Band 4 × 4 Multi-Feed Array Antenna-in-Package for High-Power Combining and Polarization Synthesis

HYUNJIN KIM, (Member, IEEE), JAEBAEK JUNG, (Student Member, IEEE), WOOJUN LEE, (Student Member, IEEE), SANGWOOK NAM, (Senior Member, IEEE), AND JUNGSUEK OH, (Senior Member, IEEE)

Department of Electrical and Computer Engineering, Institute of New Media and Communications (INMC), Seoul National University, Seoul 08826, South Korea

Corresponding author: Jungsuek Oh (jungsuek@snu.ac.kr)

This work was supported in part by the Institute of Information and Communications Technology Planning and Evaluation (IITP) Grant funded by the Korean Government through MSIT (Development of key technologies for 6G RF front-end based on low-power MIMO and highly efficient spatial QAM synthesis, 50%) under Grant 2021-0-00198; and in part by the Basic Science Research Program through the National Research Foundation of Korea (NRF) funded by the Ministry of Education under Grant 2022R1A6A3A01085999.

ABSTRACT A 4 × 4 multi-feed array antenna-in-package (AiP) is presented for high-power combinations and various polarization syntheses, which operates at D-band. The multi-feed antenna element was designed considering N-number ($K \times K$) of array antennas from the beginning. Consequently, the proposed antenna can provide four input ports while achieving an impedance bandwidth of 27%, port-to-port isolation higher than 10 dB, and cross-polarization discrimination (XPD) exceeding 20 dB. Moreover, power combination and polarization synthesis can be achieved using various excitation states. The 4 × 4 antenna array, according to simulated results, achieves a gain of up to 18.2 dBi, radiation efficiency of 81%, and XPD of over 20 dB. For verification purposes, the proposed antennas were designed with power dividers for different polarization states. An −10 dB impedance bandwidth of over 27% and a coverage of over ±60° were measured in the experiment.

INDEX TERMS D-band, multi-feed, multilayer printed PCB, antenna array.

I. INTRODUCTION

Millimeter wave (mmWave) antennas and communication systems have been researched and developed for a long time. High-mmWave frequency bands, such as the D-band, ranging from 110 to 170 GHz, have also recently received increasing attention. However, there are several challenges in realizing high-mmWave communication. One of these problems is free-space path loss, which is proportional to the square of the frequency. In addition, the effect of atmospheric absorption is typically more severe at higher frequencies than at lower frequencies [1]. Hence, many studies have been conducted to compensate for these losses, such as massive antenna arrays and power combining, suggested to achieve a higher effective isotropic radiated power (EIRP).

The associate editor coordinating the review of this manuscript and approving it for publication was Muhammad Usman Afzal.

Several studies have been conducted on multi-feed antennas that can achieve on-antenna power combinations [2], [3]. A dual-feed square-loop antenna was presented [4] to eliminate the lossy power-combining network between the transmitter and antenna. The integrated lens antenna in [5] and [6] was realized in a silicon germanium (SiGe) metal layer backend process for power combinations using an on-chip antenna. In addition, attempts have been made to codesign and cointegrate an on-chip multi-feed antenna with a low-noise amplifier (LNA) and a power amplifier (PA) [7], [8], [9]. Various multi-feed antennas were employed to achieve noise-canceling or transconductance (G_m)-boosting for the LNA and Chireix outphasing for the PA. A stacked patch antenna was proposed in [10] to provide power-combining and multiple-polarization states.

Previous studies have been based on a single antenna with multiple feeds for an on-antenna power combination,

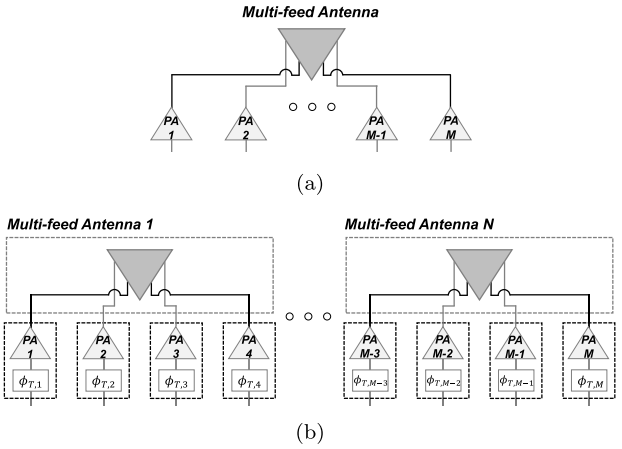

FIGURE 1. (a) Conventional single antenna with multi-feed for on-antenna power combining. (b) Proposed multi-feed array antenna configuration for on-antenna power combining.

as illustrated in Fig. 1(a) [2], [3], [4], [5]. This configuration is suitable for on-chip antennas and maintains a wide single-element beam width. However, the structure does not consider array antenna gain and beamforming, which are essential in mmWave transmitter and receiver systems. Although this configuration can provide a power combination of M PAs, it must renounce the array factor N. Previous research encountered challenges in arranging array antennas. This was primarily due to the fact that the conventional method often placed antennas and feeding networks on-chip or on-plane PCBs together with RFIC in a two-dimensional arrangement, involving intricate feeding networks for antenna element placement. This configuration consequently posed limitations in allocating space for an array setup.

We propose a multi-feed array antenna configuration for on-antenna power combination, as illustrated in Fig. 1(b). The proposed structure implements antennas and feeding networks on the AiP, creating a 3D structure by stacking the AiP over the RFIC. This difference allows for easier implementation of antenna arrays. From the beginning, the multi-feed antenna element was designed considering N-number ($K \times K$) of array antennas. Hence, the proposed antenna can provide multiple input ports while maintaining impedance bandwidth of 27%, port-to-port isolation higher than 10 dB, and cross-polarization discrimination (XPD) over 20 dB. If there are four ports in an antenna element, the array configuration can potentially provide an EIRP N^2 higher than that of a conventional single antenna with four feeds. The proposed antenna is designed as a multilayered printed circuit board (PCB) and can be interconnected using mmWave radio-frequency integrated circuits (RFIC). Most antennas for silicon-based mmWave modules are designed and integrated using a multilayered fabrication process with RFIC interconnections [11], [12], [13], [14], [15], [16], [17]. Antenna-in-package (AiP) structures enable interconnection loss reduction, effective packaging, and reliable production.

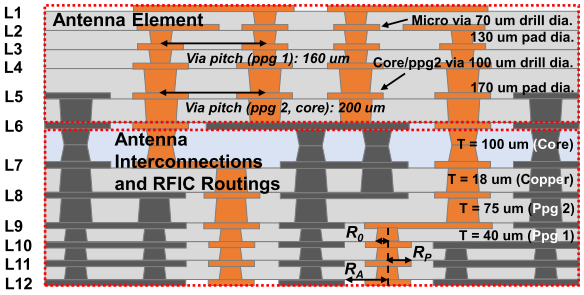

FIGURE 2. Antenna layer structure in multilayered PCB technology.

In addition, AiPs with RFIC interconnections using flip-chip bonding can be scalably extended or easily mounted on the user's equipment. The integrated design of the feeding networks in a multilayered PCB allows for array antenna configurations.

Co-linearly polarized microstrip antennas have been studied for full-duplex systems [18], [19], [20], [21]. This antenna can be used for simultaneous transmission and receiver systems that require high isolation between the transmitter and receiver. Several methods are available to achieve high antenna isolation, such as near-field cancellation [22], phase orthogonality [23], and decoupling resonators [20], [24]. However, these studies differ from ours in frequency, number of multiports, PCB fabrication process, and applications.

This paper presents a multi-feed AiP array for power combination and polarization synthesis and is organized as follows. In Section II, the geometry of the novel multi-feed antenna element design, its design procedure, operating principles, and isolation enhancing structure are presented. Section III presents the power divider design for the validation of power combining, various antenna polarization, and 4 × 4 array antenna performance. Section IV provides validation using the experimental results. Finally, Section VI presents the conclusions.

II. ANTENNA ELEMENT DESIGN

This section describes the geometry of the proposed antenna elements. In addition, the evolution process and operating principles are presented to demonstrate how the port-to-port isolation of the proposed multi-feed antenna is enhanced using shorted patch resonant modes. Fig. 2 shows the layered structure of the proposed antenna in the multilayered PCB technology. The PCB is composed of twelve copper layers and eleven dielectric layers, where the dielectrics consist of one core layer and ten layers of pre-impregnated material (prepreg or ppg), respectively. The antenna element was designed utilizing six copper layers from L1 to L6, while the remaining layers, from L6 to L12, were employed for antenna interconnections and RFIC routing. The relative dielectric permittivities of the core and prepreg substrates, ε_r, were 3.4 and 3.2, respectively, and the loss tangent was 0.004. Advanced PCB fabrication technologies can provide a minimum trace width and spacing of 30 μm. The minimum via pitch and diameters of the via and pad are shown in

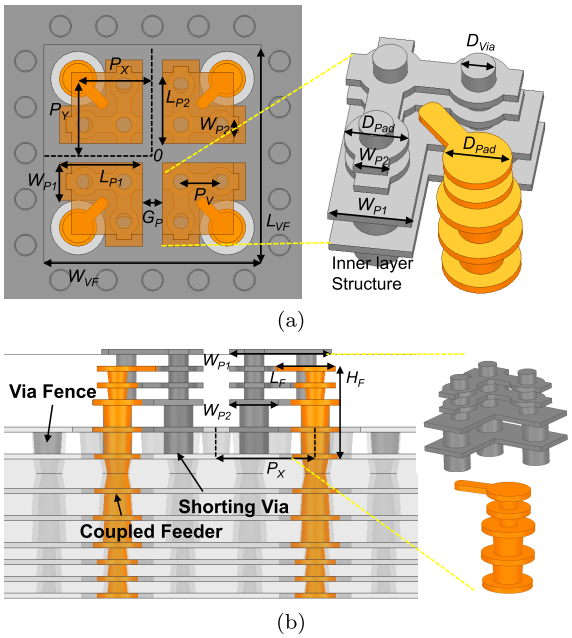

FIGURE 3. Configuration of the proposed multi-feed antenna element with shorting vias and coupled feeder. (a) Top view. (b) Cross-section view.

TABLE 1. The design parameters of the proposed antenna.

Parameters	L_{P1}	W_{P1}	L_{P2}	W_{P2}	G_P	H_F	L_F
Values (μm)	325	70	380	170	90	302	190
Parameters	P_X	P_Y	L_{VF}	W_{VF}	L_{EL}	W_{EL}	P_V
Values (μm)	340	340	990	990	1800	1800	210

Fig. 2, which varies depending on the thicknesses of the core and ppg layers. The complexity of the antenna design necessitates a sophisticated manufacturing process involving vias and lines, which can be particularly susceptible to fabrication errors. Consequently, the impact of fabrication tolerances becomes more pronounced, and achieving the desired outcome becomes progressively challenging with higher frequencies.

A. ANTENNA ELEMENT GEOMETRY

Fig. 3 shows the configuration of the proposed multi-feed antenna element with a rectangular radiating patch, shorting vias, coupled feeders, and a via fence. The ANSYS electromagnetic (EM) tool was used to design and analyze the antenna element, and the top and cross-sectional views of the model are shown in Fig. 3(a) and (b). It comprises a patch of size L_{P1} and W_{P1} and a shorting patch of size L_{P2} and W_{P2}, as shown in Fig. 3(a). The gap between the shorting vias, G_P, was determined to achieve higher isolation between the antenna ports. A monopole-type coupled feeder with a height of H_F and length of L_F, located at P_X and P_Y, is exploited to achieve a wide bandwidth. In addition, a via fence with sizes of L_{VF} and W_{VF} was used to enhance the isolation between the array antenna elements. The size of the ground plane, L_{EL} and W_{EL}, or the antenna spacing, was determined to be $0.55\lambda_0$ at the center frequency, 130 GHz. The design

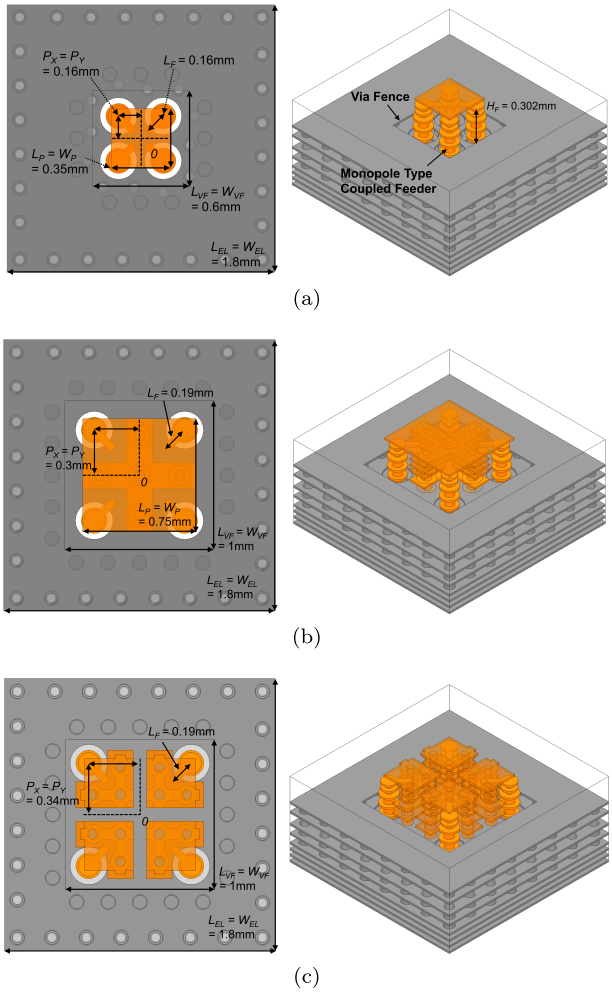

FIGURE 4. Evolution of proposed antenna. Top view and bird-eye view of (a) multi-feed antenna element with coupled feeders (Type 1). (b) shorted patch antenna element with coupled feeders (Type 2). (c) shorted patch antenna with a gap (Type 3).

parameters were elaborately adjusted to meet the design rules of multilayered PCB technology, such as the minimum trace width and spacing, via pitch, and diameter of the via and pad, as shown in Fig. 2, and achieved the best performance of the antenna element. Table 1 lists all parameters of the proposed antenna in Fig. 3.

B. ANTENNA DESIGN PROCEDURE

At the beginning of the design procedure, a coupled feed patch antenna with a length of $0.5\lambda_g$ was designed for wide bandwidth and 45° slant polarization. The configuration and dimensions of the antenna are shown in Fig. 4(a), which has a coupled feeder and via fence length of 0.6 mm. The four ports of the antennas are fed using symmetrical feeding points, where $P_X = P_Y = 0.16$ mm. The targeted bandwidth was 20 GHz (120 - 140 GHz), and impedance matching was obtained for all antennas, as shown in Fig. 5. The resonant frequencies and wavenumbers of the patch can be expressed as $m, n = 0, 1, 2\ldots$ for a rectangular patch, such as Type 1, and can be modified as

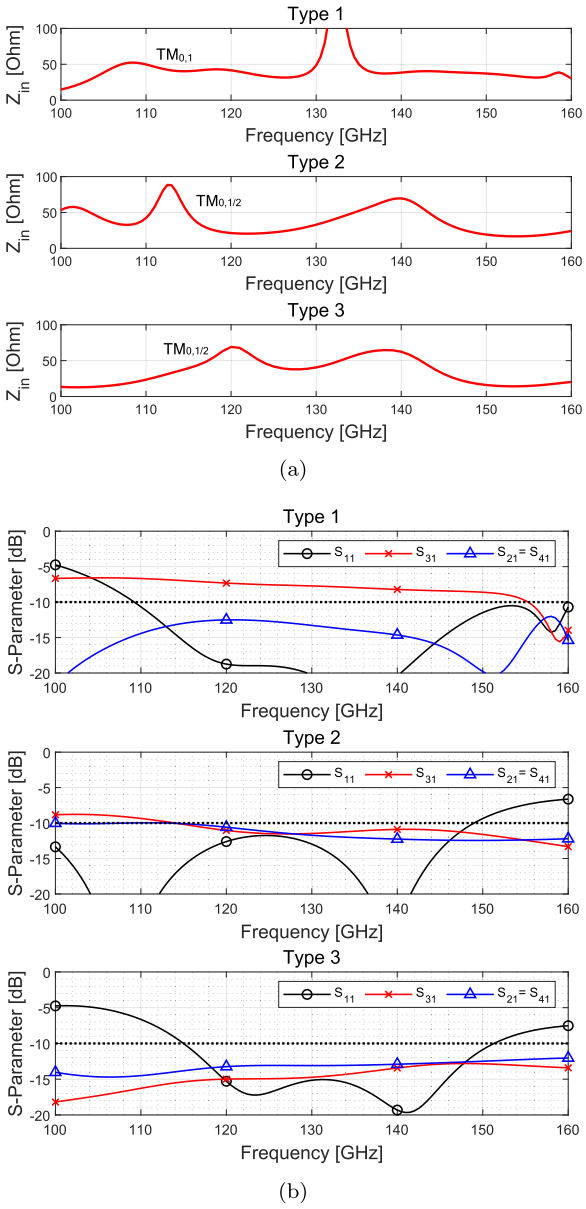

FIGURE 5. (a) Real part of input impedance of multi-feed antennas.(b) S-parameters of multi-feed antennas.

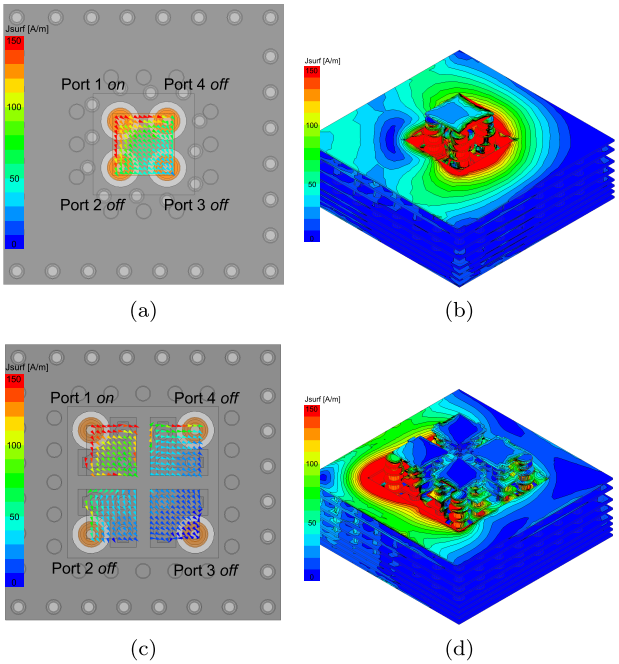

FIGURE 6. Surface current field distribution of the multi-feed antenna at 130 GHz. (a) Top view and (b) Bird-eye view of Type 1. (c) Top view and (d) Bird-eye view of Type 3.

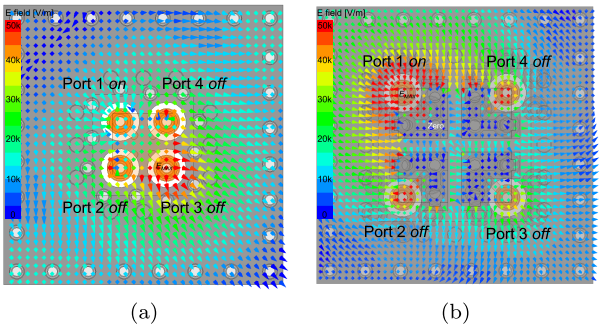

FIGURE 7. Electric field distributions of (a) Type 1 and (b) Type 3 at 130 GHz.

$m = 0, 2, 4 \ldots$, and $n = 1/2, 3/2, 5/2 \ldots$ for a shorted patch, such as Type 2 and 3. The resonant frequencies of the $TM_{0,1}$ and $TM_{0,1/2}$ modes of the antennas were adjusted to approximately 110 GHz to achieve a wide bandwidth, as shown in Fig. 5(a).

A regular microstrip antenna exhibits a strong coupling between co-linear ports (port 1-3, and port 2-4), usually with an isolation of approximately 2 dB [20]. Antenna Type 1 can achieve wide bandwidth and comparably high isolation using coupled feeders, as illustrated in Fig. 5(a) and (b). However, the targeted isolation is 10 dB because the isolation affects the active S-parameters, which are given by a linear combination of regular S-parameters [25]. Antenna Type 2 was modified with shorting vias in the center of the patch, as shown in Fig. 4(b) to achieve higher isolation. The shorting vias comprised five vias with a minimum pad diameter and a via pitch of 0.29 mm. Wider impedance matching can be achieved by using a shorted patch mode $TM_{0,1/2}$, as illustrated in Fig. 5(b) [26]. The port-to-port isolation was also improved to approximately 10 dB. For further isolation enhancement, Antenna Type 3 was proposed which has a shortened patch with a gap, as shown in Fig. 4(c). The antenna comprises four identical shorted patches with three shorting vias and a minimum via pitch of 0.2 mm. The gap between the shorted patches is 0.09 mm to keep the minimum via pitch. Although the bandwidth of S_{11} is slightly reduced, the isolation between ports S_{21}, S_{31}, and S_{41} is enhanced to approximately 13 dB at the center frequency of 130 GHz.

The antenna performance was also confirmed by surface current field distributions, as illustrated in Fig. 6. The current distributions of the top and bird's-eye views of Antenna Type 1 are shown in Fig. 6(a) and (b), when Port 1 is excited,

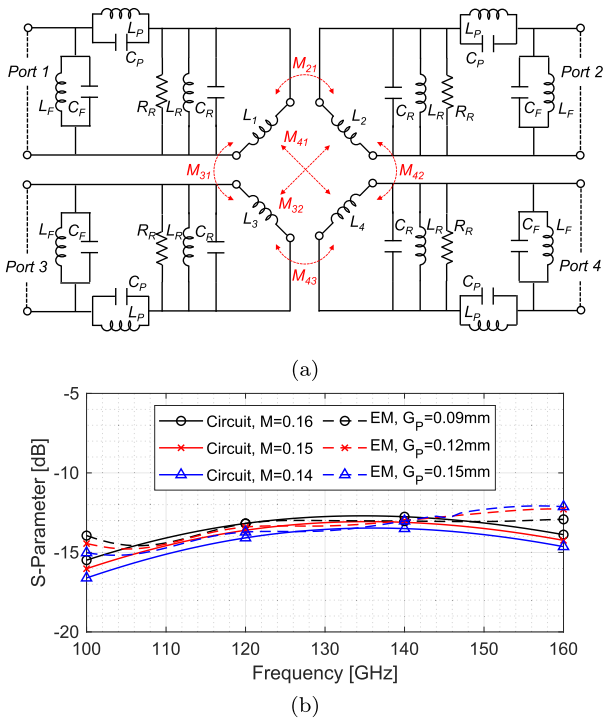

FIGURE 8. (a) Equivalent circuit model of the multi-feed patch antenna. (b) Compared S-parameters of the circuit and EM simulation.

there is a high coupling intensity between Ports 1 and 3. The electric field distribution of Antenna Type 1, illustrated in Fig. 7(a), shows the fundamental mode of the patch antenna, and the maximum field is exhibited at the opposite end of the feeder. Consequently, the mutual coupling is high because of the surface current and electric field distribution. The surface current can be reduced by the gap in the proposed antenna, which can be observed in the current distribution of Antenna Type 3, as shown in Fig. 6(c) and (d). In addition, the electric field of the shorted-patch mode, $TM_{0,1/2}$, is zero at the opposite end of the feeder, as shown in Fig. 7(b). In addition, the shorted wall can block the leakage waves between two shorted patches, and mutual coupling can be reduced.

The equivalent circuit model of the proposed multi-feed antenna is illustrated in Fig. 8(a) to demonstrate the working principles. The coupled feeder can be modeled with parallel RLC circuits, where L_F and L_P are the equivalent inductances, and C_F and C_P represent the equivalent capacitances of the feeder. The radiating patch can also be modeled with the equivalent inductance L_R, equivalent capacitance C_R, and equivalent resistance R_R. The coupling between the ports of the patch can be modeled as coupling inductors with coupling factors M. The parameters are derived through tuning within the ADS circuit simulator. In Fig. 8(b), a comparison between the circuit simulation results and the EM simulation results is presented to validate the model. The variations in S_{21} due to different G_P values are depicted, illustrating that the mutual coupling factor M decreases as G_P increases, subsequently leading to a reduction in S_{21}. This model facilitates a more straightforward investigation of port isolation.

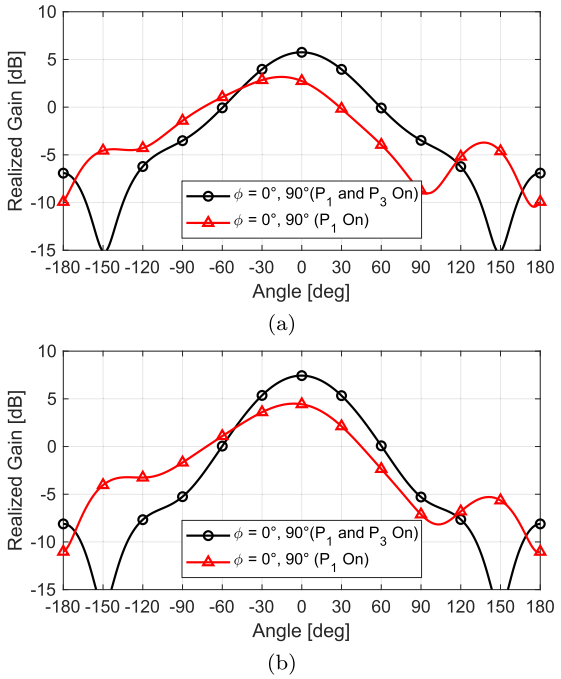

FIGURE 9. Radiation patterns of the multi-feed antenna element. (a) Type 1. (b) Type 3.

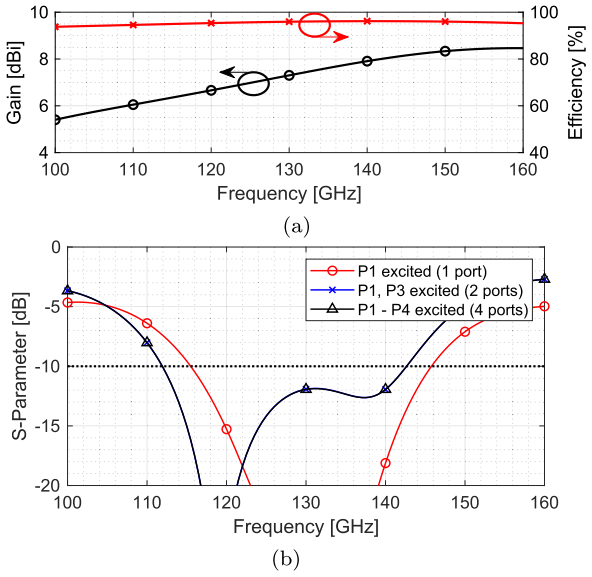

FIGURE 10. (a) Efficiency-frequency and gain-frequency curves of Antenna Type 3. (b) Active S-parameters of Antenna Type 3.

C. ANTENNA RADIATION PERFORMANCE

The radiation patterns of the multi-feed antennas are shown in Fig. 9 for various excitation states at 130 GHz. Antenna Type 1 has the current distribution and broadside radiation pattern of the $TM_{1,0}$ mode of the microstrip patch antenna, as illustrated in Fig. 9(a), which exhibits a beam squint when Port 1 is excited. However, the radiation pattern of the excitation of the two ports exhibited a higher gain of 6.3 dBi without a beam squint. By contrast, the radiation patterns shown in Fig. 9(b) show the performance of Antenna Type 3. The maximum antenna gain was 7.4 dBi with excitation

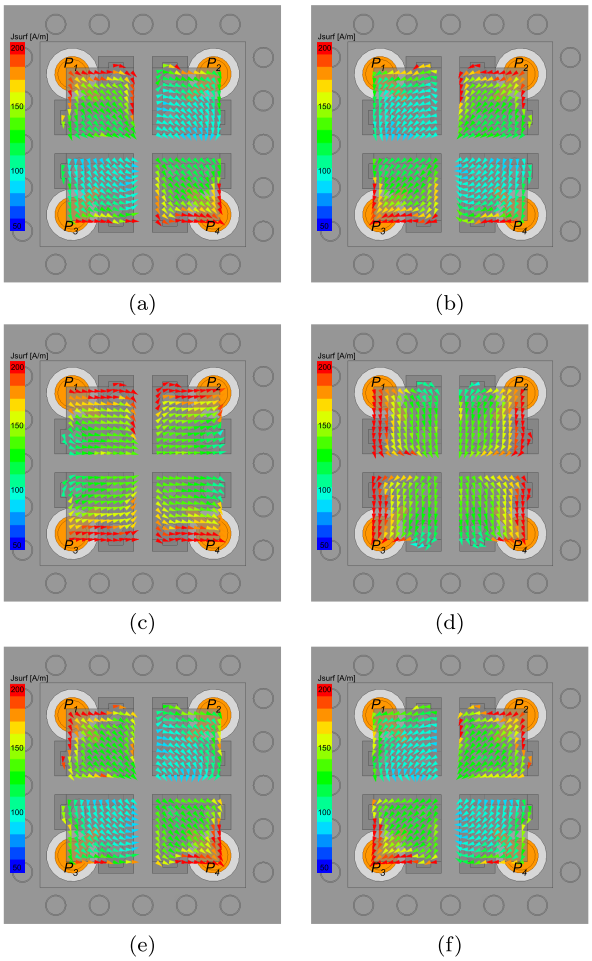

FIGURE 11. Surface current field distribution of multi-feed antenna at 130 GHz. (a) LHCP. (b) RHCP. (c) 0° LP. (d) 90° LP. (e) 45° LP. (f) −45° LP.

from the two ports, and the half-power beamwidth was approximately 72°.

The efficiency-frequency and gain-frequency curves of Antenna Type 3 are plotted in Fig. 10(a). The efficiency exceeded 90%, and the gain was above 6 dBi across all frequencies, providing coverage for the entire D-band in terms of the 3 dB gain bandwidth. The active S-parameters of Antenna Type 3 are shown in Fig. 10(b), for the three excitation states. A bandwidth of greater than 20 GHz was maintained for various excitation states. If the phases of the four ports were

$$P_3 - P_1 = (2n-1)\pi,\ P_4 - P_2 = (2n-1)\pi,\ (n = 1,\ 2, \ldots) \tag{1}$$

Then, the active S-parameter of the proposed antenna for the two ports and four ports can be obtained from

$$Active\ S_1\ (2\ ports) = \frac{a_1}{a_1}S_{11} + \frac{a_3}{a_1}S_{31} = S_{11} - S_{31} \tag{2}$$

$$\begin{aligned} Active\ S_1\ (4\ ports) &= \frac{a_1}{a_1}S_{11} + \frac{a_2}{a_1}S_{21} + \frac{a_3}{a_1}S_{31} + \frac{a_4}{a_1}S_{41} \\ &= S_{11} - S_{31} \end{aligned} \tag{3}$$

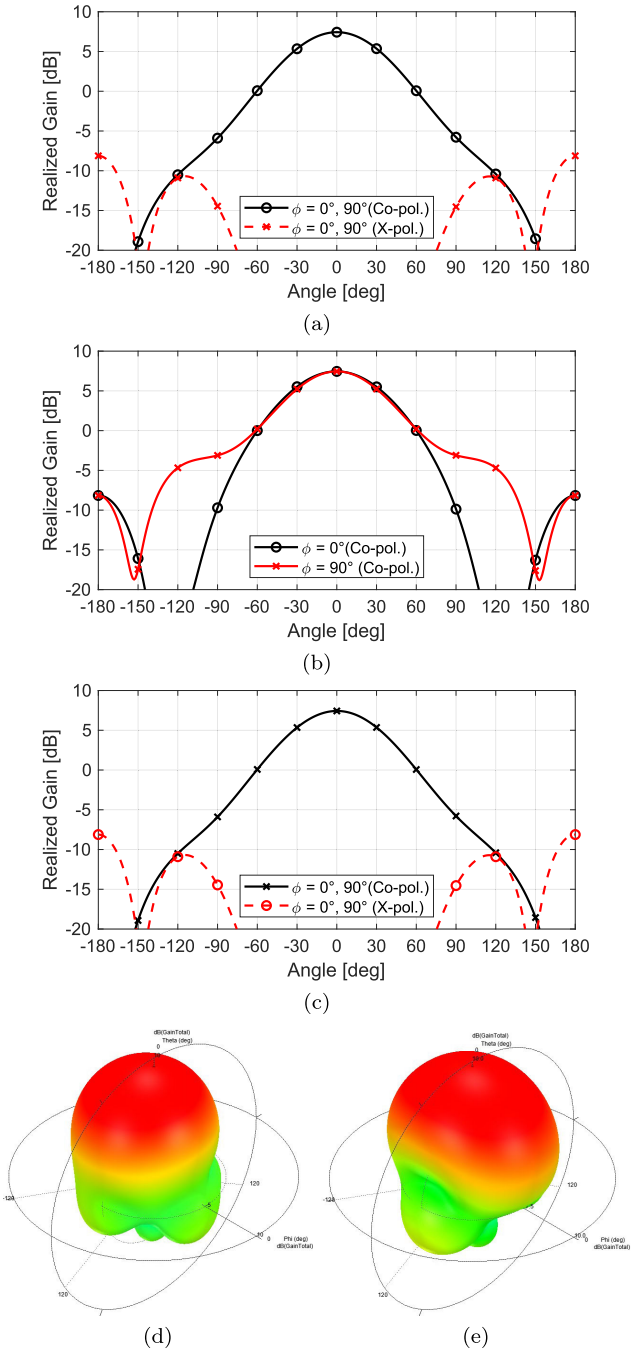

FIGURE 12. Radiation patterns for various polarization at 130 GHz. (a) LHCP. (b) 90° LP. (c) 45° LP. (d) 3D radiation pattern of LHCP. (e) 90° LP.

where matrix *Smn* is the transmission coefficient from port m to port n and a_m is the complex excitation of port m. This implies that the reflection coefficients of the proposed antenna are the same for different polarization states when (1) is satisfied, as illustrated in Fig. 10.

D. POWER COMBINING AND POLARIZATION SYNTHESIS

The proposed Type 3 multi-feed antenna provided power combinations and various polarization syntheses. By adjusting the input phases of the four ports, 0°, 90°, and ±45°

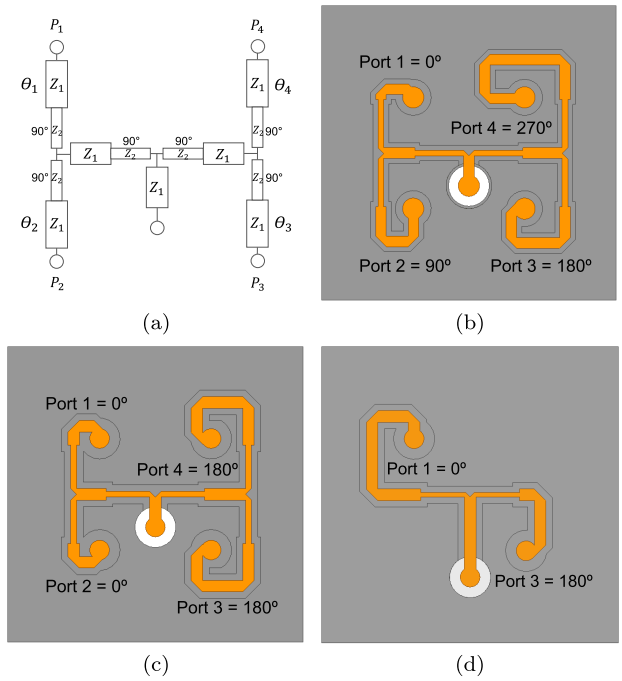

FIGURE 13. T-junction Power divider designs for various polarization. (a) Configuration of the power dividers. (b) LHCP. (c) 0° LP. (d) 45° Slant LP.

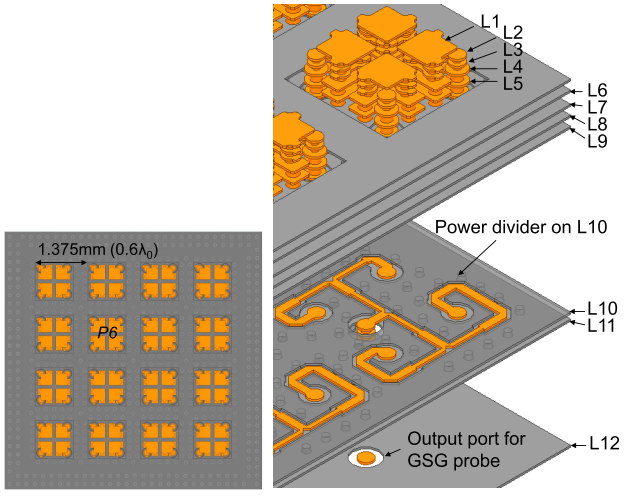

FIGURE 14. Simulation model of 4 × 4 LHCP antenna array. (a) Top view. (b) Exploded view.

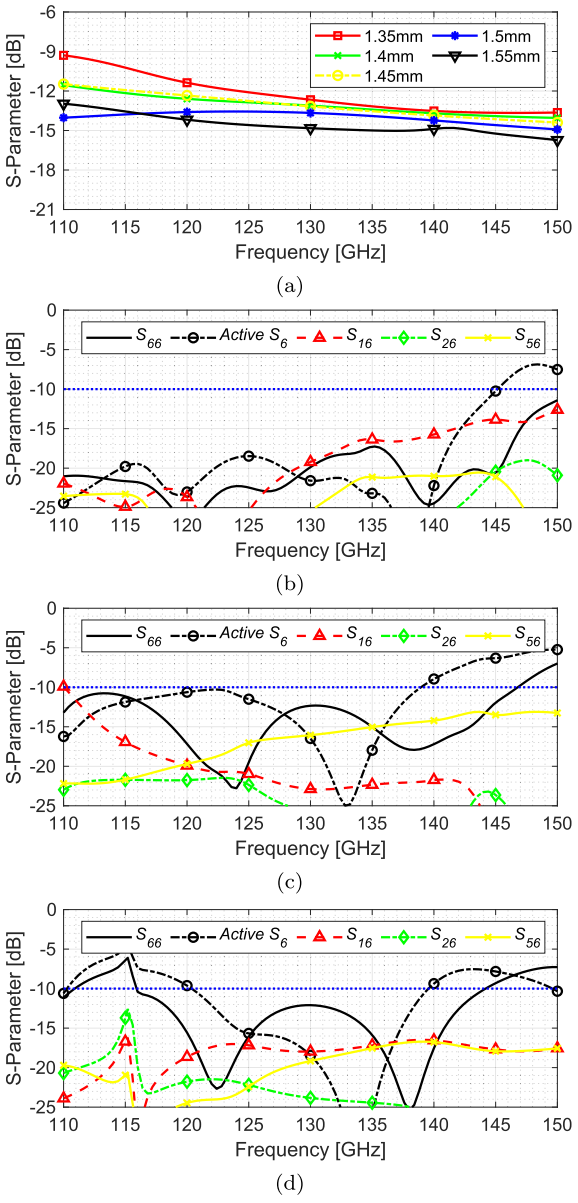

FIGURE 15. S-parameters of Port 6 in 4 × four antenna array. (a) S_{65} versus array spacing. (b) CP. (c) 0° LP. (d) 45° LP.

linear polarization (LP), left-handed circular polarization (LHCP), and right-handed circular polarization (RHCP) can be generated [10]. For example, the phases of the four ports can be controlled to obtain the CP states by using

$$P_1 = 0°,\ P_2 = 90°,\ P_3 = 180°,\ P_4 = 270° \quad (4)$$

$$P_1 = 270°,\ P_2 = 180°,\ P_3 = 90°,\ P_4 = 0° \quad (5)$$

LHCP can be generated with the states of (4), and RHCP can be obtained using (5). In Fig. 11(a) and (b), the surface current field distributions of the LHCP and RHCP can be observed in these states. Fig. 12(a) shows the radiation patterns of the LHCP, which has high gain and high XPD. A 3D radiation pattern of the LHCP is also shown in Fig. 12(d). The radiation patterns of the RHCP are the same, but the polarization is opposite to that of the LHCP.

Similarly, the LP states can be synthesized in the following phases:

$$P_1 = 0°,\ P_2 = 0°,\ P_3 = 180°,\ P_4 = 180° \quad (6)$$

$$P_1 = 0°,\ P_2 = 180°,\ P_3 = 180°,\ P_4 = 0° \quad (7)$$

Figs. 11(c) and (d) show the surface current field distributions of the 0° and 90° LP with the phase states of (6) and (7), respectively. Fig. 12(b) shows the radiation patterns of the 90° LP, and Fig. 12(b) illustrates the radiation pattern. The radiation pattern of the X-pol. could not be plotted because of their extremely high XPD values. A ±45° slant LP can

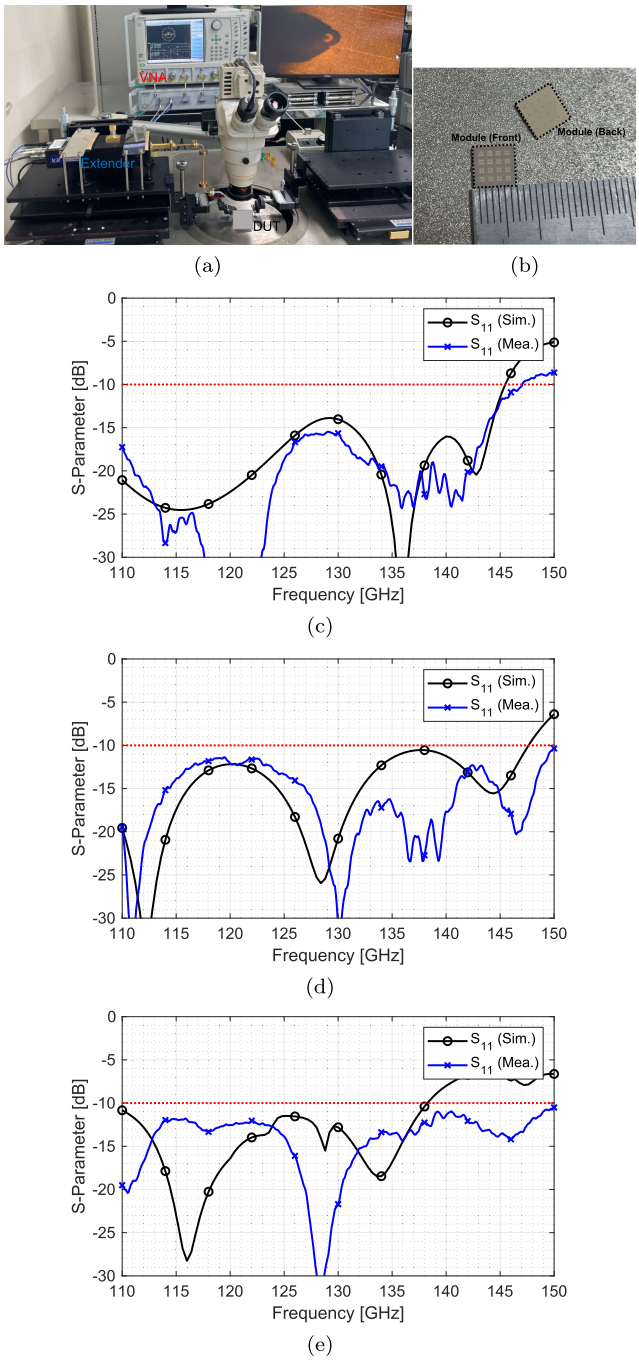

FIGURE 16. Photographs of (a) Measurement setup. (b) Fabricated modules. Compared S-parameters of (c) CP. (d) 0° LP. (e) 45° LP.

also be generated by the proposed antenna with phases of

$$P_1 = 0^\circ,\ P_2 :\ off,\ P_3 = 180^\circ,\ P_4 :\ off \quad (8)$$

$$P_1 :\ off,\ P_2 = 0^\circ,\ P_3 :\ off,\ P_4 = 180^\circ \quad (9)$$

The 45° slant LP can be synthesized with $P_1 = 0^\circ$, $P_3 = 180^\circ$, whereas P_2 and P_4 are loaded at 50Ω and the -45° slant LP can be realized with $P_2 = 0^\circ$, $P_4 = 180^\circ$, whereas P_1 and P_3 are off states. Figs. 11(e) and (f) show the surface current field distributions of the 45° and -45° LP, respectively. Fig. 12(c) shows the radiation patterns of

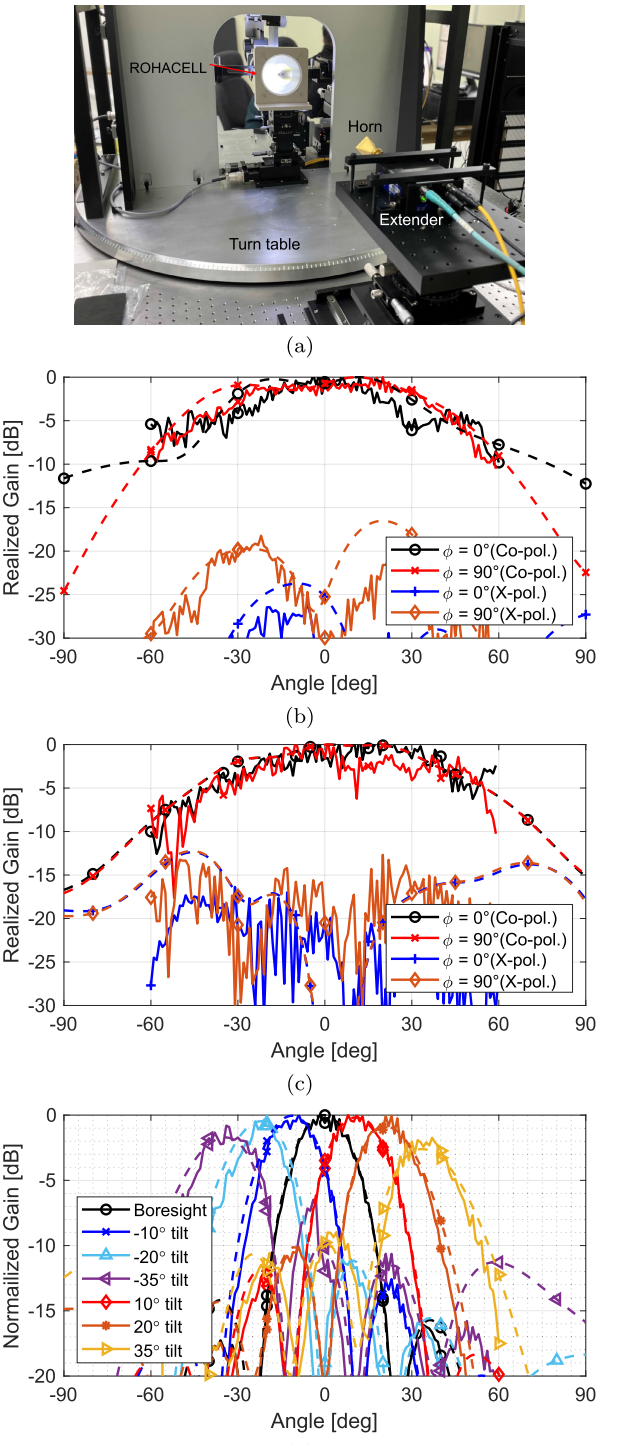

FIGURE 17. (a) Photograph of radiation pattern measurement arrangement. Compared radiation patterns of 4 × 4 array antenna.(- Measurement, - - Simulation) (b) 90° LP. (c) 45° LP. (d) Beamforming performance.

the 45° slanted LP, which were the same as those of the CP. The reflection coefficients of all the polarization states are the same, as shown in Fig. 10. With a symmetric feeder design and differential phase states, the active S parameters are the same and stable for all polarization syntheses.

TABLE 2. Comparison of multi-feed antennas.

Ref. No.	Aperture size	No. of port	f_0 (GHz)	BW (%)	Gain (dBi)	Isolation (dB)	Pol. States	Technology
[2]	$0.54\lambda_0 \times 0.54\lambda_0$ (Single)	8	161	-	4.4 (Sim.)	-	Circular	SiGe BiCMOS
[3]	$0.5\lambda_0 \times 0.5\lambda_0$ (Single)	4	134.5	35.6 (Sim.)	3 (Sim.)	-	Circular	SOI CMOS
[4]	$2.95\lambda_0 \times 1.92\lambda_0$ (Single, ground)	2	38.5 73.5	13 (Mea.) 14 (Mea.)	2.9 (Mea.) 3 (Mea.)	-	-	RO3003 LCP
[5]	- (Single)	4	245	48.9 (Mea.)	5.1 (Mea.) 24.9 (Lens, Mea.)	-	-	SiGe
[7]	$0.97\lambda_0 \times 0.97\lambda_0$ (Single, ground)	3 (Slot) 2 (Loop)	13.3	5.3 (Sim.) 16.8 (Sim.)	5.1 (Sim.) 4.5 (Sim.)	-	-	RO3003
[10]	$0.54\lambda_0 \times 0.54\lambda_0$ (Single)	4	2.5	16 (Mea.)	8.8 (Mea.)	-	4LP, 2CP	PCB
[29]	- (4 × 4)	1	140	17 (Mea.)	16.3 (Mea.)	-	-	LTCC
[30]	$2.65\lambda_0 \times 2.65\lambda_0$ (4 × 4)	1	140	55 (Sim.) 31 (Mea.)	5.5 (Sim.) 18 (Array, Sim.)	> 15	-	Layered PCB
[31]	$2\lambda_0 \times 2\lambda_0$ (4 × 4)	1	145	14 (Mea.)	14 (Mea.)	> 17	-	Layered PCB
[32]	$2.4\lambda_0 \times 2.2\lambda_0$ (4 × 4)	1	110	8 (Sim.)	13.5 (Sim.)	> 20	-	SiGe Superstrate
This work	$2.4\lambda_0 \times 2.4\lambda_0$ (4 × 4)	4	130	27 (Mea.)	8.6 (Sim.) 18.2 (Array, Sim.)	> 13	4LP, 2CP	Layered PCB

III. EXPERIMENTAL VALIDATION

A. DESIGN FOR VALIDATION

The polarization states of the proposed antenna array can be achieved by adjusting the phase shifters of the RF front-ends, as illustrated in Fig. 1(b). As presented in Fig. 13, three power dividers were designed instead of phase shifters to verify the power-combining and polarization-synthesizing operations of the proposed multi-feed antenna. Power dividers with different output phases have been used to replace phase shifters [27], [28], as shown in the configuration of the power dividers in Fig. 13(a). The phase of the power divider, ranging from θ_1 to θ_4, was adjusted by controlling the length of the lines, and three states-LHCP, 0° LP, and 45° LP-were designed, as illustrated in Fig. 13(b), (c), and (d). For 45° slant LP divider as shown in Fig. 13 (d), the two remaining ports (port 2 and port 3) are not connected and are left open. The power dividers are located in Layer 10 of the multilayered PCB, as shown in Fig. 2. Subsequently, 4 × 4 antenna arrays were designed and fabricated to verify array performance for three different polarization states. The top view and the exploded view of the simulation model of the 4 × 4 LHCP antenna array is shown in Fig. 14(a) and (b). The element spacing was determined to be 1.375 mm, approximately $0.6\lambda_0$ at 130 GHz. Fig. 15 shows the simulated S-parameters of the antenna array. Isolation between antenna elements, S_{65}, decreases with increasing array spacing, as shown in Fig. 15(a). The reflection coefficients, active S-parameter, and isolation of Port 6 are plotted for various polarization states, as shown in Fig. 15(b), (c), and (d). Although the antenna elements are the same, the S-parameters differ depending on the type of power divider and the polarization state.

B. S-PARAMETER MEASUREMENTS

A photograph of the measurement setup used for the validation is shown in Fig. 16(a). The measurement setup comprised a vector network analyzer (VNA), waveguide-connected ground-signal-ground (GSG) probes, and a frequency extension unit. The extension unit expanded the operating frequency of the VNA from 110 GHz to 170 GHz. Three types (CP, 0° LP, and 45° LP) of 4 × 4 antenna array modules are fabricated, as illustrated in Fig. 16(b) to verify the antenna designs described in the previous sections. The modules were measured on ROHACELL foam, and the measured S-parameters were similar to the measured results, as shown in Fig. 16(c), (d), and (e). S_{11} of the measured results achieved a bandwidth of approximately 35 GHz (27%) for various types of polarization states.

C. RADIATION PATTERN VALIDATION

The setup for measuring the radiation pattern is shown in Fig. 17(a), which is a vertically mountable measurement setup for D-band frequencies that incorporates waveguide, frequency extension units, and a VNA with GSG probes. The calibration board and device under test can be vertically installed on ROHACELL foam, allowing for both calibration and radiation pattern measurements. The horn antenna is fixed as shown in Fig. 17(a), and the measurement angle

could be automatically adjusted from −60° to 60° using a turn table. The radiation patterns of the antenna elements are plotted at 130 GHz for $\phi = 0°$ and 90° (the E and H planes) in Fig. 17. The normalized radiation patterns with the maximum gain are plotted with Fig. 17(b) LHCP and (c) 90° LP, and the results are similar to the simulated results. The radiation patterns of the 4 × 4 antenna array are shown in Fig. 17(d). Element gains were measured at each port, and the measured gains were synthesized to verify the beamforming characteristics. The sidelobe level of 4 × 4 antenna array exceeds 15 dB. A coverage of more than ±50° was measured in the experiment. The array radiation pattern from simulated results could also achieve a gain of up to 18.2 dBi, radiation efficiency of 81%, and XPD of over 20 dB.

D. COMPARISON WITH PREVIOUS STUDIES

Table 1 compares the performance of the proposed antenna with those of previously studied multi-feed antennas. The figure of merit was evaluated based on the aperture size, the number of antenna arrays, the number of multiports, center frequency, −10 dB impedance bandwidth, maximum antenna gain, multi-feed isolation between antenna elements, available polarization states, and fabrication technology. The proposed antenna array has an impedance bandwidth of more than 27%, which is relatively wide compared with those reported in previous studies. In addition, the maximum gain here is higher than that of other antennas, which is caused by the antenna element configuration and array of antennas. Compared to a single feed 4 × 4 array antenna operating at D-band frequency [29], [30], [31], [32], [33], the proposed antenna demonstrates a higher array gain. Additionally, there is a potential expectation of a 6 dB increase in EIRP due to power combining.

IV. CONCLUSION

A 4 × 4 array AiP is presented for high-power combination and polarization synthesis using a multi-feed configuration, which operates at D-band. The multi-feed antenna element was designed by considering four input ports while maintaining the impedance bandwidth of 27%, port-to-port isolation higher than 10 dB, and XPD over 20 dB. The configuration is anticipated to result in a 6 dB higher EIRP compared to a conventional single feed 4 × 4 array antenna. In addition, the power combination and polarization synthesis can be achieved using various excitation states. A 4 × 4 antenna array from simulated results achieves a gain of up to 18.2 dBi, radiation efficiency of 81%, and XPD of over 20 dB. The proposed antennas were designed with power dividers for different polarization states for verification purposes. An −10 dB impedance bandwidth of 27% and coverage of over ±50° were measured in the experiment.

REFERENCES

[1] G. A. Siles, J. M. Riera, and P. Garcia-del-Pino, "Atmospheric attenuation in wireless communication systems at millimeter and THz frequencies," *IEEE Antennas Propag. Mag.*, vol. 57, no. 1, pp. 48–61, Feb. 2015.

[2] S. M. Bowers and A. Hajimiri, "Multi-port driven radiators," *IEEE Trans. Microw. Theory Techn.*, vol. 61, no. 12, pp. 4428–4441, Dec. 2013.

[3] S. M. Bowers, A. Safaripour, and A. Hajimiri, "An integrated slot-ring traveling-wave radiator," *IEEE Trans. Microw. Theory Techn.*, vol. 63, no. 4, pp. 1154–1162, Apr. 2015.

[4] S. Li, T. Chi, Y. Wang, and H. Wang, "A millimeter-wave dual-feed square loop antenna for 5G communications," *IEEE Trans. Antennas Propag.*, vol. 65, no. 12, pp. 6317–6328, Dec. 2017.

[5] B. Goettel, P. Pahl, C. Kutschker, S. Malz, U. R. Pfeiffer, and T. Zwick, "Active multiple feed on-chip antennas with efficient in-antenna power combining operating at 200–320 GHz," *IEEE Trans. Antennas Propag.*, vol. 65, no. 2, pp. 416–423, Feb. 2017.

[6] J. G. Marin, A. A. Baba, J. Hesselbarth, R. M. Hashmi, and K. P. Esselle, "Millimeter-wave low-loss multifeed superstrate-based antenna," *IEEE Trans. Antennas Propag.*, vol. 68, no. 5, pp. 3387–3396, May 2020.

[7] T. Chi, S. Li, J. S. Park, and H. Wang, "A multifeed antenna for high-efficiency on-antenna power combining," *IEEE Trans. Antennas Propag.*, vol. 65, no. 12, pp. 6937–6951, Dec. 2017.

[8] S. Li, T. Chi, J.-S. Park, H. T. Nguyen, and H. Wang, "A 28-GHz flip-chip packaged Chireix transmitter with on-antenna outphasing active load modulation," *IEEE J. Solid-State Circuits*, vol. 54, no. 5, pp. 1243–1253, May 2019.

[9] S. Li, T. Chi, and H. Wang, "Multi-feed antenna and electronics co-design: An E-band antenna-LNA front end with on-antenna noise-canceling and G_m-boosting," *IEEE J. Solid-State Circuits*, vol. 55, no. 12, pp. 3362–3375, Dec. 2020.

[10] W. Duan, X. Y. Zhang, S. Liao, K. X. Wang, and Q. Xue, "Multiport power combining patch antenna with stable reflection coefficient and radiation pattern in six polarization states," *IEEE Trans. Antennas Propag.*, vol. 67, no. 2, pp. 719–729, Feb. 2019.

[11] X. Gu, D. Liu, and B. Sadhu, "Packaging and antenna integration for silicon-based millimeter-wave phased arrays: 5G and beyond," *IEEE J. Microw.*, vol. 1, no. 1, pp. 123–134, Jan. 2021.

[12] J. Seo, I. Yoon, J. Jung, J. Ryoo, J. Park, W. Lee, D. Ko, and J. Oh, "Miniaturized dual-band broadside/endfire antenna-in-package for 5G smartphone," *IEEE Trans. Antennas Propag.*, vol. 69, no. 12, pp. 8100–8114, Dec. 2021.

[13] H. Kim and S. Nam, "Performance enhancement of 5G millimeter wave antenna module integrated tablet device," *IEEE Trans. Antennas Propag.*, vol. 69, no. 7, pp. 3800–3810, Jul. 2021.

[14] Y. Kim, H. Kim, I. Yoon, and J. Oh, "4 × 8 patch array-fed FR4-based transmit array antennas for affordable and reliable 5G beam steering," *IEEE Access*, vol. 7, pp. 88881–88893, 2019.

[15] T. Joo, C. Hwang, J. Park, K. Kim, and J. Jung, "Design of a tile-type Rx multi-beam digital active phased array antenna system," *J. Electromagn. Eng. Sci.*, vol. 22, no. 1, pp. 12–20, Jan. 2022.

[16] A. Altaf, M. Elahi, S. M. Abbas, J. Yousaf, and E. Almajali, "A D-band waveguide-SIW transition for 6G applications," *J. Electromagn. Eng. Sci.*, vol. 22, no. 4, pp. 419–426, Jul. 2022.

[17] H. Kim, Y. Lee, B. Kim, K. Baek, S. Ko, T. Yang, J. Lee, and S. Nam, "60 GHz digitally controllable and sequentially rotated fed antenna array," *Electron. Lett.*, vol. 53, no. 13, pp. 821–822, Jun. 2017.

[18] O. N. Alrabadi, A. D. Tatomirescu, M. B. Knudsen, M. Pelosi, and G. F. Pedersen, "Breaking the transmitter–receiver isolation barrier in mobile handsets with spatial duplexing," *IEEE Trans. Antennas Propag.*, vol. 61, no. 4, pp. 2241–2251, Apr. 2013.

[19] H. Nawaz and I. Tekin, "Dual-polarized, differential fed microstrip patch antennas with very high interport isolation for full-duplex communication," *IEEE Trans. Antennas Propag.*, vol. 65, no. 12, pp. 7355–7360, Dec. 2017.

[20] Y. He and Y. Li, "Compact co-linearly polarized microstrip antenna with fence-strip resonator loading for in-band full-duplex systems," *IEEE Trans. Antennas Propag.*, vol. 69, no. 11, pp. 7125–7133, Nov. 2021.

[21] R. Zaker and A. Kheirdoost, "Bandwidth and isolation improvement of highly coupled printed array antenna using multiple shorting posts," *IEEE Trans. Antennas Propag.*, vol. 69, no. 11, pp. 7987–7992, Nov. 2021.

[22] J. Wu, M. Li, and N. Behdad, "A wideband, unidirectional circularly polarized antenna for full-duplex applications," *IEEE Trans. Antennas Propag.*, vol. 66, no. 3, pp. 1559–1563, Mar. 2018.

[23] M. R. Nikkhah, J. Wu, H. Luyen, and N. Behdad, "A concurrently dual-polarized, simultaneous transmit and receive (STAR) antenna," *IEEE Trans. Antennas Propag.*, vol. 68, no. 8, pp. 5935–5944, Aug. 2020.

[24] N.-W. Liu, Y.-D. Liang, L. Zhu, G. Fu, Y. Liu, and Y. Yun, "Electric-field null bending of a single dual-port patch antenna for colinear polarization decoupling using characteristic modes analysis," *IEEE Trans. Antennas Propag.*, vol. 70, no. 12, pp. 12247–12252, Dec. 2022.
[25] C. X. Bai, Y. J. Cheng, Y. R. Ding, and J. F. Zhang, "A metamaterial-based S/X-band shared-aperture phased-array antenna with wide beam scanning coverage," *IEEE Trans. Antennas Propag.*, vol. 68, no. 6, pp. 4283–4292, Jun. 2020.
[26] N.-W. Liu, L. Zhu, Z.-X. Liu, Z.-Y. Zhang, G. Fu, and Y. Liu, "Cross-polarization reduction of a shorted patch antenna with broadside radiation using a pair of open-ended stubs," *IEEE Trans. Antennas Propag.*, vol. 68, no. 1, pp. 13–20, Jan. 2020.
[27] H. Yi, E. Ozturk, M. Koelink, J. Krimmling, A. A. Damian, W. Debski, H. W. van Zeijl, G. Zhang, and R. H. Poelma, "Antenna-in-package (AiP) using through-polymer vias (TPVs) for a 122-GHz radar chip," *IEEE Trans. Compon., Packag., Manuf. Technol.*, vol. 12, no. 6, pp. 893–901, Jun. 2022.
[28] B. Zhang, H. Gulan, T. Zwick, Y. Li, U. Oderfält, F. Carlsson, and H. Zirath, "Integration of a 140 GHz packaged LTCC grid array antenna with an InP detector," *IEEE Trans. Compon., Packag., Manuf. Technol.*, vol. 5, no. 8, pp. 1060–1068, Aug. 2015.
[29] J. Xu, Z. N. Chen, X. Qing, and W. Hong, "140-GHz planar broadband LTCC SIW slot antenna array," *IEEE Trans. Antennas Propag.*, vol. 60, no. 6, pp. 3025–3028, Jun. 2012.
[30] H. Kim and J. Oh, "140-GHz wideband array antenna-in-package using multimode resonance," *IEEE Trans. Antennas Propag.*, vol. 71, no. 3, pp. 2136–2144, Mar. 2023.
[31] A. Lamminen, J. Säily, J. Ala-Laurinaho, J. de Cos, and V. Ermolov, "Patch antenna and antenna array on multilayer high-frequency PCB for D-band," *IEEE Open J. Antennas Propag.*, vol. 1, pp. 396–403, 2020.
[32] W. Shin, B.-H. Ku, O. Inac, Y.-C. Ou, and G. M. Rebeiz, "A 108–114 GHz 4 × 4 wafer-scale phased array transmitter with high-efficiency on-chip antennas," *IEEE J. Solid-State Circuits*, vol. 48, no. 9, pp. 2041–2055, Sep. 2013.
[33] M. de Kok, A. B. Smolders, and U. Johannsen, "A review of design and integration technologies for D-band antennas," *IEEE Open J. Antennas Propag.*, vol. 2, pp. 746–758, 2021.

HYUNJIN KIM (Member, IEEE) received the B.S. degree in electronic engineering from Korea University, Seoul, South Korea, in 2006, and the M.S. and Ph.D. degrees in electrical engineering from Seoul National University, Seoul, in 2009 and 2021, respectively. From 2009 to 2020, he was a Staff Engineer with Samsung Electronics, Suwon, where he was responsible for research on advanced antenna technologies for communications, advanced network devices, and mmWave antenna systems. He is currently a Postdoctoral Research Fellow with the Department of Electrical and Computer Engineering, Institute of New Media and Communications, Seoul National University. His research interests include D-band antenna design, mmWave array antenna systems, and metasurfaces.

JAEBAEK JUNG (Student Member, IEEE) received the B.S. degree in electronic and electrical engineering from the Pohang University of Science and Technology (POSTECH), Pohang, South Korea, in 2012. He is currently pursuing the integrated master's and Ph.D. degree with the Department of Electrical Engineering and Computer Science, Seoul National University, Seoul, South Korea. His research interests include mmWave 5G antenna, 6G antenna, metasurface, and antenna in package.

WOOJUN LEE (Student Member, IEEE) received the B.S. and M.S. degrees in electrical and computer engineering from Seoul National University, South Korea, in 2021 and 2023, respectively. He is currently pursuing the Ph.D. degree in electrical and computer engineering with Virginia Tech, Blacksburg, VA, USA. His current research interests include inverse design in electromagnetics, active integrated antenna, and RFIC.

SANGWOOK NAM (Senior Member, IEEE) received the B.S. degree in electrical engineering from Seoul National University, Seoul, South Korea, in 1981, the M.S. degree in electrical engineering from the Korea Advanced Institute of Science and Technology (KAIST), Daejeon, South Korea, in 1983, and the Ph.D. degree in electrical engineering from The University of Texas at Austin, Austin, TX, USA, in 1989. From 1983 to 1986, he was a Researcher with the Gold Star Central Research Laboratory, Seoul. Since 1990, he has been a Professor with the School of Electrical Engineering and Computer Science, Seoul National University. His research interests include the analysis/design of electromagnetic structures, antennas, and microwave active/passive circuits.

JUNGSUEK OH (Senior Member, IEEE) received the B.S. and M.S. degrees from Seoul National University, South Korea, in 2002 and 2007, respectively, and the Ph.D. degree from the University of Michigan, Ann Arbor, in 2012. From 2007 to 2008, he was with Korea Telecom as a Hardware Research Engineer, working on the development of flexible RF devices. In 2012, he was a Postdoctoral Research Fellow with the Radiation Laboratory, University of Michigan. From 2013 to 2014, he was a Staff RF Engineer with Samsung Research America, Dallas, working as a Project Leader for the 5G/millimeter-wave antenna systems. From 2015 to 2018, he was a Faculty Member with the Department of Electronic Engineering, Inha University, South Korea. He is currently an Associate Professor with the School of Electrical and Computer Engineering, Seoul National University. He has published over 50 technical journals and conference papers. His research interests include mmWave beam focusing/shaping techniques, antenna miniaturization for integrated systems, and radio-propagation modeling for indoor scenarios. He has served as a TPC Member and the Session Chair for the IEEE AP-S/USNC-URSI and ISAP. He was a recipient of the 2011 Rackham Predoctoral Fellowship Award at the University of Michigan. He has served as a Technical Reviewer for IEEE TRANSACTIONS ON ANTENNAS AND PROPAGATION and IEEE ANTENNA AND WIRELESS PROPAGATION LETTERS.